This document is the post-print version of a submitted work that was subsequently accepted for publication in International Journal of Heat and Mass Transfer. To access the published version:
https://doi.org/10.1016/j.ijheatmasstransfer.2021.121247

# Thermal contact resistance evaluation of a thermoelectric system by means of three *I-V* curves

Braulio Beltrán-Pitarch*, Francisco Vidan, and Jorge García-Cañadas

*Department of Industrial Systems Engineering and Design, Universitat Jaume I, Campus del Riu Sec, 12006 Castellón, Spain*

**e-mail: beltranb@uji.es*

To achieve a suitable performance in a thermoelectric (TE) device it is important to minimize the thermal contact resistances between the device external surfaces and the heat exchangers of the system (heat source and heat sink). Despite its relevance, there are not many methods available for the evaluation of the thermal contact resistance, and the existing ones typically employ complex setups. Here, we present a new method to determine the thermal contact resistance of a TE device thermally contacted to a heat sink and a heat source. The method is based on performing three current-voltage (*I-V*) curves at different system conditions under a small temperature difference. First, an *I-V* curve with a high voltage scan rate, which avoids the variation of the initial temperature difference, provides the ohmic resistance. A second *I-V* curve performed with a constant input heat power (or the device suspended) provides the TE resistance. Finally, a third *I-V* curve with a constant temperature difference between the heat exchangers allows obtaining the thermal contact resistance. Using this method, a thermal contact resistivity value of $3.57 \times 10^{-4}$ $m^2KW^{-1}$ was obtained for a commercial Bi-Te TE module contacted with a heat source and a heat sink using thermal grease as thermal contact interface material, which is in good agreement with reported values. The new method is highly advantageous, since neither involves complex setups nor requires the measurement of heat fluxes. Moreover, it measures directly under operating conditions for small temperature differences.

Keywords: Thermal interface, thermal contact resistance, heat exchangers, *I-V* curve, measurement techniques, current-voltage characteristics

## I. INTRODUCTION

When a thermoelectric (TE) device works under operating conditions, converting a heat flux into electrical energy, it is sandwiched between a heat source and a heat sink (heat exchangers). The conversion efficiency of the device not only depends on the TE properties of the TE legs, but it also depends on the temperature gradient across

them. Considering the second case, it is important to keep the temperature difference between the two sides of the TE legs as similar as possible to the temperature difference between the heat source and heat sink to maximize the conversion efficiency. The main contribution to the discrepancy between both temperature differences is the thermal contact resistance [1] that exists at the interface between the heat exchangers and the typical ceramics that act as insulating layers of a TE module. Hence, it is crucial to characterize and minimize the thermal contact resistance.

Usually, the thermal contact resistance between two solids is measured by the determination of the temperature drop produced at the interface of the materials in contact and the heat flux flows across the junction. This method usually involves the use of several thermocouples and materials with known thermal conductivity [2–6]. In other cases, it is also common to use an infrared camera instead of thermocouples to determine the temperature profile across the junction [7,8]. Furthermore, we have recently showed how impedance spectroscopy can determine this parameter when a TE device is contacted by heat sinks [9].

*I-V* curves are typically used to characterize a wide range of devices (e.g. thin film transistors [10], strained carbon nanotubes [11], photovoltaic cells [12], and solar concentrators [13]). An *I-V* curve typically consists of varying the voltage of a device while the current flowing through it is recorded. The *I-V* curve can be performed at different voltage scan rates, which could be useful to identify processes occurring at different time scales. In a TE device, a sufficiently high voltage scan rate only shows the ohmic resistance of the device, since the fast voltage variation does not allow a variation of the initial temperature profile. The way to experimentally determine this voltage scan rate will be described in the *Experimental Results* section. On the other hand, an *I-V* curve performed waiting for different steady state *I* and *V* values allows the temperature variations induced by the Peltier effect to contribute to the response. These different *I-V* curves have been demonstrated to be useful for the determination of the figure of merit *zT* of a TE device [14], and the total thermal parasitic resistance [15,16]. However, none of these methods allowed the independent determination of the thermal contact resistance.

In this work, we show how the thermal contact resistance between a TE module and the heat source/sink can be independently obtained by means of *I-V* curves. In addition, the module figure of merit *zT*, and the total ohmic resistance of the TE device can be also determined. This new approach can be very useful for TE module characterization and, specially, for the analysis and optimization of the unavoidable thermal contacts, which play a key role in the efforts to maximize the heat to electricity energy conversion efficiency of a TE system.

## II. METHOD PRINCIPLE

The new method is based on the different thermal profiles that exist in a TE device sandwiched between a heat source and a heat sink under three different conditions. The system is modeled as shown in Fig. 1. In this model, the TE module is simplified by a cylindrical TE leg of length $L$ in contact with two cylindrical layers (one at each end) of length $L_C$ that simulate their ceramic plates. The use of cylindrical legs has been shown to have no significant

differences with respect to a prismatic geometry, and it simplifies the thermal spreading-constriction analysis [17]. The thermal influence of the thin copper strips that contact the TE legs with the ceramics is neglected due to their small thickness and high thermal conductivity. The system is assumed to be under adiabatic conditions. Joule effect and the variation with temperature of the TE properties are discarded, since the initial temperature difference between heat source and heat sink and the current flowing through the device are considered to be small. In any case, this assumption will be experimentally tested in the *Experimental Results* section. Finally, a perfect thermal contact between the ceramics and the TE legs is considered.

Fig. 1 shows schematically the temperature profiles of the system under three different conditions compared with the initial (open-circuit) state. Fig. 1(a) shows the profile obtained for a constant heat power heat source and a perfect heat sink. The former can be experimentally achieved by, for example, powering cartridge heaters of a heat source with a constant current and voltage. Under this condition, temperature in the heat sink does not change when current is varied, but the temperature in the heat source decreases until a new steady state is reached due to the cooling produced by the Peltier effect at $x$=0, being $x$ the position. Since the input heat power is constant, at steady state all the heat injected at the cold junction ($x$=$L$) by the Peltier effect (current flow) becomes cancelled by the reduction in the heat flow reaching this junction from the TE element. This heat flow reduction is produced by the cooling experienced at the hot junction ($x$=0) by the Peltier effect as well. This happens for any constant current flowing through the TE module.

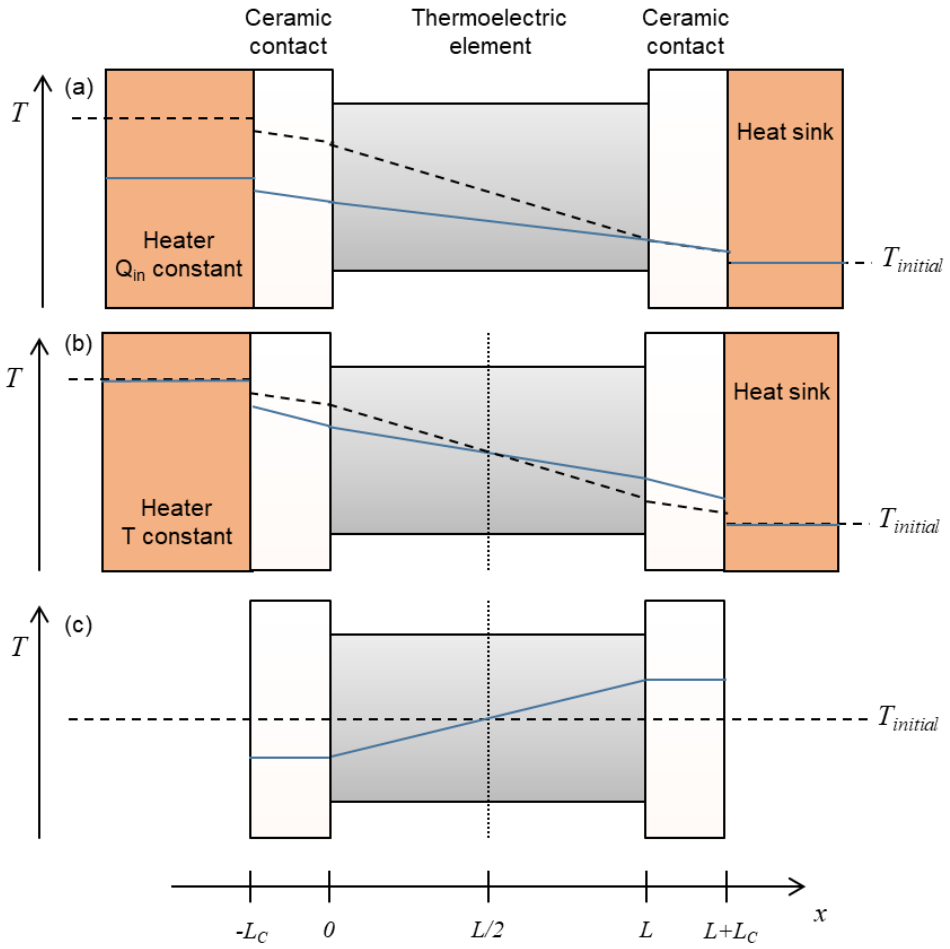


Fig. 1. Schematics of steady-state temperature profiles in a TE module attached to a heat source and a heat sink under an initial temperature difference (dashed line), and after a constant current flow is present or varied (solid blue line). (a) Case of a constant heat power input $Q_{in}$ for a small initial temperature difference [e.g. $T(x<-L_C)$-$T(x>L+L_C)$=10 K] and (b) case of a constant temperature difference [same value as in (a)] between heat exchangers. (c) is the case for a suspended module in vacuum with no heat exchangers attached and an initial constant temperature which is the average of cases (a) and (b). Positive electrical current and Seebeck coefficient are considered.

Fig. 1(b) shows the temperature profile for a constant temperature heat source and a perfect heat sink, that is, constant temperature difference between the heat exchangers. The temperature in the heat source and the heat sink do not change when the current flows through the TE device, however, inside the TE module, temperature varies due to the current since the hot side ($x$=0) of the TE legs is cooled down and the cold side ($x$=$L$) is heated up because of the Peltier effect. Notice that, at steady state, the temperature drops across the ceramics and at the ceramics/heat exchangers interfaces increases in case (b) with respect to the initial temperature profile, which was not the case in Fig. 1(a), where it remained constant.

Additionally, Fig. 1(c) shows the temperature profile generated in a TE module suspended in vacuum and without the presence of heat exchangers. In this case, as in the constant heat input case, once the steady state is reached, all the heat generated at one side of the TE legs by the Peltier effect is eventually removed at the other side for any constant current flow.

The potential difference $V$=$V(L)$-$V(0)$, of a TE module is given by,

$$V = R_{\Omega} I - 2NS\Delta T_{TE}, \quad (1)$$

where $N$ is the number of couples of the TE module, $S$ is the average absolute Seebeck coefficient of a TE leg, $\Delta T_{TE}=T(L)-T(0)$ is the temperature difference between the cold and hot sides of the TE legs, $R_{\Omega}$ is the total ohmic resistance of the device, which includes the contribution of wires, TE legs, copper strips, and all electrical contacts between these elements. $I$ is the current extracted from the device. It should be noticed that under these considerations a *p*-type leg ($S>0$) will show a positive open-circuit voltage and a positive current will be extracted under closed circuit. Hence, the slope of the *I-V* curve should be negative, consequently, the resistance will show a negative value. Thus, although resistances are typically considered positive, we will keep its negative sign in our derivations in order to be consistent with the physical meaning (negative slope).

Since an *I-V* curve performed to a TE device typically follows a straight line, the latter can be defined by the straight-line equation $V=V_{oc}+R_{IV}I$, being $V_{oc}$ the open-circuit voltage and $R_{IV}$ the slope of the *I-V* curve. Since the voltage defined by this equation should be equal to that defined in Eq. (1), this allows obtaining the slope of the *I-V* curve (notice that $V_{oc}=-2NS\Delta T_{TE,oc}$, where $\Delta T_{TE,oc}$ is the temperature difference between the cold and hot sides at open circuit),

$$R_{IV} = R_{\Omega} - 2NS\frac{\left(\Delta T_{TE} - \Delta T_{TE,oc}\right)}{I} = R_{\Omega} - 2NS\frac{\Delta T_P}{I}, \quad (2)$$

being $\Delta T_P$ the variation of the temperature difference with respect to the open-circuit value. It can be seen from Eq. (2) that the slope of the *I-V* curve is governed by two contributions, (i) the total ohmic resistance of the TE device, and (ii) a term that is influenced by the current, the number of legs, the Seebeck coefficient, and the variation of the open-circuit temperature difference that is produced due to the Peltier effect.

As shown in Eq. (2), the total ohmic resistance of the TE module can be obtained from an *I-V* curve performed at a high enough voltage scan rate, able to avoid the variation of the open-circuit temperature difference, leading in this case to,

$$R_{IV} = R_{\Omega}. \quad (3)$$

Hence, a first *I-V* curve can be performed under this condition, allowing the determination of the total ohmic resistance of the TE module independently of the boundary conditions of the system.

A second measurement allows the determination of the TE resistance of the TE module by means of an *I-V* curve performed under constant heat power input $Q_{in}$. In this *I-V* curve the different points should be obtained at steady state conditions, i.e. the current and voltage values should be recorded once they become constant after varying the load resistance. For a TE module sandwiched between a constant heat power heat source and a perfect heat sink [Fig. 1(a)], the energy balance at $x=0$ is given by,

$$-ST_0I = \frac{\lambda_C A_C}{L_C}\Delta T_C - \frac{\lambda_{TE} A_{TE}}{L}\Delta T_{TE}, \quad (4)$$

where $\lambda_C$, $A_C$, $\lambda_{TE}$, and $A_{TE}$ are the average thermal conductivity and area of the ceramic layers and TE legs, respectively, and $\Delta T_C = T(0) - T(-L_C)$ is the temperature difference across the ceramics. $T_0 = T(0)$ can be approximated as the average initial temperature (at open circuit), $T_0 \approx [T(L)_{oc} + T(0)_{oc}]/2$. Since $Q_{in}$ is constant, it can be found from the energy balance at $x = -L_C$ at open circuit and under constant current flow conditions that the temperature difference across the ceramic layer does not change ($\Delta T_C = \Delta T_{C,oc}$, where $\Delta T_{C,oc}$ is the temperature drop across the ceramics at open-circuit condition). On the other hand, the temperature drop across the TE elements may be defined as the addition of the open-circuit and Peltier contributions ($\Delta T_{TE} = \Delta T_{TE,oc} + \Delta T_P$). Then, Eq. (4) can be rewritten as,

$$-ST_0I = \frac{\lambda_C A_C}{L_C}\Delta T_{C,oc} - \frac{\lambda_{TE} A_{TE}}{L}\Delta T_{TE,oc} - \frac{\lambda_{TE} A_{TE}}{L}\Delta T_P. \quad (5)$$

Since at open-circuit condition the heat flowing through the ceramic layer is the same than the heat flowing through the TE legs,

$$\frac{\lambda_C A_C}{L_C}\Delta T_{C,oc} = \frac{\lambda_{TE} A_{TE}}{L}\Delta T_{TE,oc}. \quad (6)$$

Eq. (5) can be simplified to,

$$ST_0I = \frac{\lambda_{TE} A_{TE}}{L}\Delta T_P, \quad (7)$$

and rearranging, we obtain the change in the temperature difference across the TE legs,

$$\Delta T_P = \frac{ST_0IL}{\lambda_{TE} A_{TE}}. \quad (8)$$

Notice that Eq. (8) is also valid for a TE module suspended in vacuum [Fig. 1(c)], since $\Delta T_C = 0$ as a consequence of the adiabatic condition and of the initial temperature profile being homogeneous ($\Delta T_{C,oc} = \Delta T_{TE,oc} = 0$). Thus, the variation of the temperature difference across the TE legs with respect to open circuit is the same for a TE module suspended in vacuum than for a module sandwiched between a constant heat power input heat source and a heat sink. Hence, performing a second *I-V* curve with the module suspended and without heat exchangers will provide the same result as the constant heat power input case, which can be experimentally beneficial, since it avoids the need of a power source able to supply constant heat power. Such an equipment might not be always available.

Introducing Eq. (8) into Eq. (2), we obtain,

$$R_{IV} = R_\Omega + R_{TE}. \quad (9)$$

where $R_{TE}$ is a TE resistance [18] and takes the form,

$$R_{TE} = -\frac{2NS^2T_0L}{\lambda_{TE}A_{TE}}. \quad (10)$$

Notice that the module $zT=R_{TE}/R_{\Omega}$, can thus be obtained from these two *I-V* curves, as previously reported [14].

Finally, a third *I-V* curve can allow the characterization of the thermal contacts. Again, like in the previous case, all the points of the curve should be obtained after reaching steady state once the load resistance is varied. For a TE module sandwiched between a constant temperature heat source and a perfect heat sink [Fig. 1(b)], now $Q_{in}=-\lambda_C A_C \Delta T_C/L_C$ changes with respect to the open-circuit value $Q_{in,oc}=-\lambda_C A_C \Delta T_{C,oc}/L_C$, being the heat power variation,

$$\Delta Q_{in} = Q_{in} - Q_{in,oc} = \frac{\lambda_C A_C}{L_C}\Delta T_{C,oc} - \frac{\lambda_C A_C}{L_C}\Delta T_C. \quad (11)$$

Using Eq. (11) in the energy balance at $x$=0 [Eq. (4)], we obtain,

$$-ST_0I = \frac{\lambda_C A_C}{L_C}\Delta T_{C,oc} - \frac{\lambda_{TE} A_{TE}}{L}\Delta T_{TE,oc} - \frac{\lambda_{TE} A_{TE}}{L}\Delta T_P - \Delta Q_{in}, \quad (12)$$

Which using Eq. (6) becomes,

$$ST_0I = \frac{\lambda_{TE} A_{TE}}{L}\Delta T_P + \Delta Q_{in}. \quad (13)$$

Introducing Eq. (13) into Eq. (2) we obtain the slope of the *I-V* curve for this third case,

$$R_{IV} = R_{\Omega} - \frac{2NS^2T_0L}{\lambda_{TE}A_{TE}} + \frac{2NSL}{\lambda_{TE}A_{TE}I}\Delta Q_{in}, \quad (14)$$

where now an additional term influenced by $\Delta Q_{in}$ appears with respect to the case of constant heat power input [Eq. (9)]. In order to obtain $\Delta Q_{in}$ a system of equations is required. These equations are obtained from different energy balances at different positions at open circuit and under current flow conditions.

Since the additional heat power that crosses the heater/ceramic interface is the same than the heat power that crosses the ceramic and the ceramic/TE interface, this system of equations to obtain $\Delta Q_{in}$ can be formulated:

$$\Delta Q_{in} = -\frac{A_C}{r_{TC}}\Delta T_{P,C,-L_C}, \quad (15)$$

$$\Delta Q_{in} = \frac{\left(\Delta T_{P,C,-L_C} - \Delta T_{P,C,0}\right)\lambda_C A_C}{L_C}, \quad (16)$$

$$\Delta Q_{in} = \frac{\left(\Delta T_{P,C,0} - \Delta T_{P,TE,0}\right)A_{TE}}{r_{S/C}}, \quad (17)$$

where $\Delta T_{P,C,-L_C}$, and $\Delta T_{P,C,0}$ are the temperature difference with respect to the open-circuit value at positions $x$=-$L_C$, and $x$=0, respectively, in the ceramic layer, which is induced by the Peltier effect. $\Delta T_{P,TE,0}$ is the temperature

increase due to the Peltier effect in the TE materials at position $x$=0, which is equal to $-\Delta T_P/2$ due to symmetry, $r_{TC}$ is the thermal contact resistivity between the TE module and the heat source/sink, and $r_{S/C}$ is the thermal spreading-constriction resistivity defined by [19],

$$r_{S/C} = r_{TC-TE} + \frac{4}{\lambda_C}\sum_{n=1}^{\infty}\frac{{J_1}^2(\delta_n\frac{r_0}{r_1})r_1}{{\delta_n}^3{J_0}^2(\delta_n)}\left[\frac{\delta_n + \frac{r_1}{r_{TC}\lambda_C}\tanh(\delta_n\frac{L_C}{r_1})}{\delta_n\tanh\left(\delta_n\frac{L_C}{r_1}\right)+\frac{r_1}{r_{TC}\lambda_C}}\right], \tag{18}$$

where $r_{TC-TE}$ is the thermal contact resistivity between the TE legs and the ceramic layers (neglected in this case), $J_0$, and $J_1$ are the Bessel functions of first kind of orders zero and one, respectively, $r_0$, and $r_1$ are the radii of the TE legs and its corresponding ceramic bits, respectively, and the eigenvalues $\delta_n$ are roots of $J_1(\delta_n) = 0$. In addition to $r_{TC\text{-}TE}$=0, when $L_C$>$r_1$, this expression can be approximated to,

$$r_{S/C} = \frac{4}{\lambda_C}\sum_{n=1}^{\infty}\frac{{J_1}^2(\delta_n\frac{r_0}{r_1})r_1}{{\delta_n}^3{J_0}^2(\delta_n)}, \tag{19}$$

which does not include $r_{TC}$, so there is no need to know its value beforehand [20].

After some algebraic steps, $\Delta Q_{in}$ is obtained as a function of $\Delta T_P$,

$$\Delta Q_{in} = \frac{\Delta T_P}{2}\left(\frac{L_C}{\lambda_C A_C} + \frac{r_{TC}}{A_C} + \frac{r_{S/C}}{A_{TE}}\right)^{-1}, \tag{20}$$

and introducing it into Eq. (13) we obtain,

$$ST_0 I = \frac{\lambda_{TE}A_{TE}}{L}\Delta T_P + \left(\frac{L_C}{\lambda_C A_C} + \frac{r_{TC}}{A_C} + \frac{r_{S/C}}{A_{TE}}\right)^{-1}\frac{\Delta T_P}{2}. \tag{21}$$

Finally, rearranging the terms,

$$\frac{\Delta T_P}{I} = ST_0\left[\frac{\lambda_{TE}A_{TE}}{L} + \left(\frac{2L_C}{\lambda_C A_C} + \frac{2r_{TC}}{A_C} + \frac{2r_{S/C}}{A_{TE}}\right)^{-1}\right]^{-1}. \tag{22}$$

Introducing Eq. (22) into Eq. (2) we obtain:

$$R_{IV} = R_\Omega + \left[{R_{TE}}^{-1} + (R_C + R_{TC} + R_{S/C})^{-1}\right]^{-1}, \tag{23}$$

where $R_C$, $R_{TC}$, and $R_{S/C}$ take the form:

$$R_C = -\frac{4NS^2T_0L_C}{\lambda_C A_C}, \tag{24}$$

$$R_{TC} = -\frac{4NS^2T_0r_{TC}}{A_C}, \quad (25)$$

$$R_{S/C} = -\frac{4NS^2T_0r_{S/C}}{A_{TE}}. \quad (26)$$

It should be noticed that $[R_{TE}^{-1}+(R_C+R_{TC}+R_{s/c})^{-1}]^{-1}<R_{TE}$, hence the third *I-V* curve will show a smaller absolute value of the slope than the second curve, although larger than the first case. In contrast to the constant heat power input case, in the curve performed under constant temperature difference between heat exchangers (third curve) the properties of the thermal contacts (ceramics layers, thermal contacts and spreading/constriction) influence the electrical response measured, since affect the additional heat injection from the heat source required when its temperature is decreased ($\Delta Q_{in}$). When this heat injection is not present, the *I-V* curve slope is only governed by the properties of the TE legs [see Eq. (14)], as in the constant heat power input and suspended module cases [Eq. (9)].

Since $R_\Omega$ and $R_{TE}$ can be extracted from the first and second *I-V* curves, respectively, now $R_C$, $R_{TC}$, and $R_{S/C}$ are unknown quantities. However, if $S$ and $\lambda_C$ are known in addition to the module architecture and $T_0$, $r_{TC}$ can be extracted from the slope of the third *I-V* curve. This will be experimentally performed in the next section. Notice that the method could be extended to high temperatures as soon as all the measurements are performed at the same initial temperatures and employing small temperature differences. The initial homogeneous temperature for the module suspended [case of Fig. 1(c)] should be the same as the mean temperature in the other configurations.

## III. EXPERIMENTAL RESULTS

The setup used in this study to perform the different *I-V* curves is schematically shown in Fig. 2. It is formed by a heat sink, which consists in circulating water through a spiral machined inside a copper block. The water was circulated using a thermostatic circulating bath (Selecta, Frigiterm TFT). The heat sink was attached to the bottom of a commercial 40 mm x 40 mm Bi-Te TE module from European Thermodynamics (Ref. 693-7080). The module is formed by 127 couples of 1.3 mm x 1.3 mm x 1.2 mm legs and 0.7 mm alumina ceramic thickness. At the other side of the TE module another copper block with the same area as the module and several cartridge heaters was contacted and served as the heat source. The heaters were powered by a variable transformer (RS, ref. 890-2872) with a fixed current and voltage when the constant heat power input condition was desired, or by a temperature controller (Watlow, EZ Zone PM) when a constant temperature difference condition was required. A thin layer of heat sink compound (thermal grease) from RS (Ref. 217-3835) was placed in the two interfaces of the TE module and the heat source/sink.

In order to test that the influence of the Joule effect is negligible, impedance spectroscopy measurements at different current amplitudes were performed to the TE module (see Fig. S2). It can be observed that the measurements nearly overlap. Only at the magnification at high frequencies (inset of Fig. S2) an increase of the

high frequency intercept (ohmic resistance) with the real axis can be observed. This can be attributed to the variation of the ohmic resistance caused by the Joule effect. However, the variation between the intercepts at 50 mA and 250 mA is only 0.3% and hence Joule effect can be considered negligible.

All the *I-V* curves were performed under a small initial temperature difference (9.2±0.1 K) across the TE module. In order to avoid differences due to the dependence of the TE properties with temperature, the average initial temperature of all the experiments was similar (26.75 and 26.65 ºC for the constant heat power input and the constant temperature difference conditions, respectively). This small temperature gradient produced small currents, which avoids significant Joule effect and also the variation of TE properties. The temperature difference was measured with two K-type thermocouples. One of them was placed inside a small hole in the heat source and the other in a groove on the heat sink. Both of them were surrounded by thermal grease for suitable thermalization. All measurements were carried out under vacuum conditions with a pressure $<1.0\text{x}10^{-4}$ mbar inside a metallic vacuum chamber, which also acted as Faraday cage, using a PGSTAT204 potentiostat equipped with a FRA32M impedance analyzer module (Metrohm Autolab B. V.). The fast *I-V* curve was performed at a 100 V/s scan rate. In order to identify this value, we performed several measurements at different scan rates (from 0.01 to 100 V/s, which is the highest allowed by the equipment) at an ambient temperature of 26.6 ºC. For each of these *I-V* curves we determined the slope, which is plotted as a function of the scan rate in Fig. S1. The most suitable scan rate is the one where variations of the slope values become nearly constant. As observed in Fig. S1, although a constant value is not completely reached, 100 V/s is the most suitable, since it is the highest allowed by the equipment and variations of the slope value are the smallest.

The other two *I-V* curves needed, in addition to the fast curve, were obtained by fixing different current values and recording the voltage once the steady state was achieved. This is equivalent to using different load resistances, the potentiostat acts as a variable load. The fast *I-V* curve was performed at the same average temperature as the constant temperature difference case (26.6 ºC).

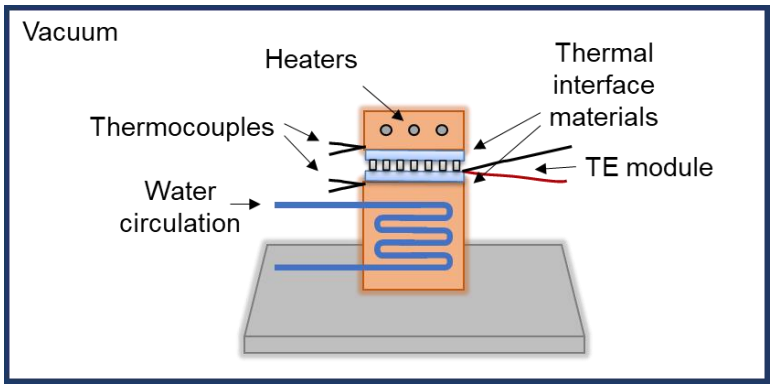


Fig. 2. Schematic of the experimental setup used to perform different *I-V* curves to a TE module.

Apart from the measurements performed to the module sandwiched between the heat exchangers (Fig. 2), an *I-V* curve and an impedance measurement was also carried out to the same module under suspended conditions in

vacuum. This *I-V* curve was also performed by fixing different current values and recording the voltage once the steady state was achieved. The impedance spectroscopy measurement was carried out at 0 A dc current and 50 mA ac amplitude with 40 points logarithmically distributed from 2 mHz to 2 kHz. Both measurements were performed at an initial ambient temperature (26.80 ºC) similar to the average temperature of the previous *I-V* curves.

Fig. 3(a) shows the four *I-V* curves performed in this study. It can be observed that the absolute value of the slope of the fast *I-V* curve is the smallest (1.172 Ω), since it is only governed by the ohmic resistance of the TE device. The constant heat power input and suspended measurements show the highest absolute values of the slopes (2.009 and 2.059 Ω, respectively), since they are governed by the ohmic resistance and the TE resistance contribution. Finally, the constant heat exchangers temperature difference measurement shows an intermediate absolute value of the slope, due to the presence of $R_C$, $R_{TC}$, and $R_{S/C}$ in addition to the TE resistance. It should be noticed that the curve corresponding to the module suspended in vacuum basically shows the same slope as the constant heat power input case. All these observations agree with the analysis in the previous section.

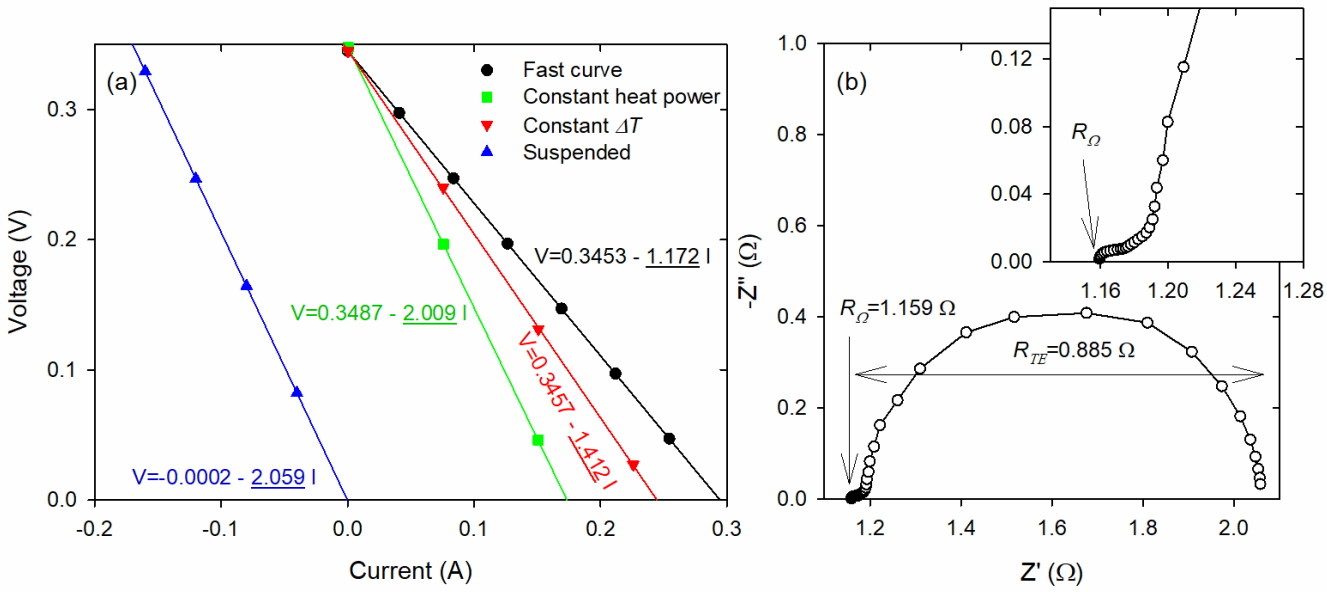


Fig. 3. (a) *I-V* curves performed to a commercial TE module at a very high scan rate (circles), at constant temperature difference between heat exchangers (down triangles), at constant heat power input heat source (squares), and suspended (up triangles). Solid lines represent the fittings to linear equations, which are also shown. (b) Impedance spectroscopy measurement of the TE module under suspended conditions. All the measurements were performed in vacuum.

Fig. 3(b) shows the impedance spectroscopy measurement performed to the same TE module. An impedance spectroscopy measurement performed to a TE module suspended in vacuum provides the total ohmic resistance $R_\Omega$ of the TE module from the high frequency intercept with the real axis. Note that frequency decreases from the left to the right side of Fig. 3(b). The TE resistance $R_{TE}$ can be also obtained from the impedance spectrum as the difference between the low and high frequency intercepts [see Fig. 3(b)] [21]. The total absolute value of the ohmic resistance $R_\Omega$ of the TE module obtained from the slope of the *I-V* curve in Fig. 3(a) performed at high scan rate (1.172 Ω) is in good agreement with the impedance spectroscopy result (1.159 Ω). Moreover, the TE resistance $R_{TE}$

absolute value (0.837 Ω), determined from the slope of the *I-V* curve performed under constant heat power input condition and the ohmic resistance of the fast *I-V* curve, as shown in Eq. (9), also agrees well with the impedance spectroscopy measurement (0.885 Ω). Practically the same result can be obtained using the *I-V* curve performed in suspended conditions ($R_{TE}$=0.887 Ω) instead of the one under constant heat power condition. The figure of merit *zT* of the TE module can be obtained as $zT=R_{TE}/R_{\Omega}$, which provided a value of 0.714 (or 0.757 using the suspended *I-V* curve).

Regarding the *I-V* curve performed with the constant temperature heat source condition, ($R_C+R_{TC}+R_{S/C}$) was obtained from its slope and using the already determined values of $R_{\Omega}$ and $R_{TE}$ employing Eq. (23). The $R_C$ (0.016 Ω) and $R_{S/C}$ (0.0188 Ω) absolute values were obtained using the dimensions of the TE module, the average Seebeck coefficient of the TE legs, and the thermal conductivity of the ceramics at room temperature (37 $WK^{-1}m^{-1}$ for alumina) [22], leading to a $R_{TC}$ absolute value of 0.302 Ω. Finally, the thermal contact resistivity $r_{TC}$, was calculated using Eq. (25) and the mentioned properties. The Seebeck coefficient of the TE module was obtained from the slope of an open-circuit voltage vs. temperature difference curve, obtaining a value of 186.42 $\mu VK^{-1}$. A thermal contact resistivity value of $3.57x10^{-4}$ $m^2KW^{-1}$ was obtained, which is in good agreement with typically reported values [5,9,23,24]. This proves the suitability of this method to determine this parameter directly under operating conditions for small temperature differences.

## IV. CONCLUSIONS

A new method using three *I-V* curves has been presented for the determination of the thermal contact resistance between a TE module and heat exchangers. In addition to this parameter, the method also allows the determination of the device total ohmic resistance and *zT*. An *I-V* curve performed with a high enough voltage scan rate allows extracting the total ohmic resistance $R_{\Omega}$ of the TE module. A second *I-V* curve carried out with a constant heat power input condition, or the module suspended in vacuum, allows the measurement of the TE resistance $R_{TE}$, and hence the figure of merit determination $zT=R_{TE}/R_{\Omega}$. Finally, a third *I-V* curve carried out with a constant temperature heat source condition allows obtaining the thermal contact resistivity $r_{TC}$, provided the module architecture, the average Seebeck coefficient of the TE legs, and the thermal conductivity of the ceramics are known. The method was experimentally tested with a commercial Bi-Te module in contact with a heat source and a heat sink using thermal grease as thermal interface material. The total ohmic resistance $R_{\Omega}$, the figure of merit *zT*, and the thermal contact resistivity obtained (1.172 Ω, 0.714, and $3.57x10^{-4}$ $m^2KW^{-1}$, respectively) agree with impedance spectroscopy measurements and literature reported values. The new method is highly beneficial, since it does not involve complex setups and allows direct measurements under operating conditions for small temperature differences.

## ACKNOWLEDGMENTS

The authors acknowledge financial support from the Spanish Agencia Estatal de Investigación under the Ramón y Cajal program (RYC-2013-13970), from the Generalitat Valenciana and the European Social Fund under the ACIF program (ACIF/2018/233), from the Universitat Jaume I under the project UJI-A2016-08, and the technical support of Raquel Oliver Valls and José Ortega Herreros. European Thermodynamics Ltd. is also acknowledged for providing the TE modules.

## REFERENCES

[1] Bergman TL, Lavine AS, Incropera FP, Dewitt DP. Fundamentals of Heat and Mass Transfer, seventh edition. 2011.

[2] Rosochowska M, Balendra R, Chodnikiewicz K. Measurements of thermal contact conductance. J Mater Process Technol 2003;135:204–10. doi:10.1016/S0924-0136(02)00897-X.

[3] Azuma K, Hatakeyama T, Nakagawa S. Measurement of surface roughness dependence of thermal contact resistance under low pressure condition. 2015 Int. Conf. Electron. Packag. iMAPS All Asia Conf., IEEE; 2015, p. 381–4. doi:10.1109/ICEP-IAAC.2015.7111040.

[4] Misra P, Nagaraju J. Test facility for simultaneous measurement of electrical and thermal contact resistance. Rev Sci Instrum 2004;75:2625–30. doi:10.1063/1.1775316.

[5] Xian Y, Zhang P, Zhai S, Yuan P, Yang D. Experimental characterization methods for thermal contact resistance: A review. Appl Therm Eng 2018;130:1530–48. doi:10.1016/j.applthermaleng.2017.10.163.

[6] Catalan L, Aranguren P, Araiz M, Perez G, Astrain D. New opportunities for electricity generation in shallow hot dry rock fields: A study of thermoelectric generators with different heat exchangers. Energy Convers Manag 2019;200:112061. doi:10.1016/J.ENCONMAN.2019.112061.

[7] Fieberg C, Kneer R. Determination of thermal contact resistance from transient temperature measurements. Int J Heat Mass Transf 2008;51:1017–23. doi:10.1016/J.IJHEATMASSTRANSFER.2007.05.004.

[8] Warzoha RJ, Donovan BF. High resolution steady-state measurements of thermal contact resistance across thermal interface material junctions. Rev Sci Instrum 2017;88:094901. doi:10.1063/1.5001835.

[9] Beltrán-Pitarch B, Vidan F, García-Cañadas J. Characterization of thermal contacts between heat exchangers and a thermoelectric module by impedance spectroscopy. Appl Therm Eng 2019:114361. doi:10.1016/J.APPLTHERMALENG.2019.114361.

[10] Chen B-W, Yu EK, Chang T-C, Kanicki J. Physical origin of the non-linearity in amorphous In-Ga-Zn-O thin-film transistor current-voltage characteristics. Solid State Electron 2018;147:51–7. doi:10.1016/J.SSE.2018.06.001.

[11] Majid MJ. I–V characteristics and conductance of strained SWCNTs. Phys Lett A 2019;383:879–87. doi:10.1016/J.PHYSLETA.2018.12.003.

[12] Hafez HS, Shenouda SS, Fadel M. Photovoltaic characteristics of natural light harvesting dye sensitized solar cells. Spectrochim Acta Part A Mol Biomol Spectrosc 2018;192:23–6. doi:10.1016/J.SAA.2017.10.066.

[13] Almonacid F, Rodrigo P, Fernández EF. Determination of the current–voltage characteristics of concentrator systems by using different adapted conventional techniques. Energy 2016;101:146–60. doi:10.1016/J.ENERGY.2016.01.082.

[14] Min G, Singh T, Garcia-Cañadas J, Ellor R. Evaluation of Thermoelectric Generators by I – V Curves. J Electron Mater 2016;45:1700–4. doi:10.1007/s11664-015-4180-z.

[15] McCarty R, Piper R. Voltage–Current Curves to Characterize Thermoelectric Generators. J Electron Mater 2015;44:1896–901. doi:10.1007/s11664-014-3585-4.

[16] Kim DH, Kim C, Kim JT, Yoon DK, Kim H. Method for evaluating interfacial resistances of thermoelectric devices using I-V measurement. Meas J Int Meas Confed 2018;129:281–7. doi:10.1016/j.measurement.2018.07.030.

[17] Muzychka Y, Culham R, Yovanovich M. Thermal Spreading Resistances in Rectangular Flux Channels: Part I Geometric Equivalences, American Institute of Aeronautics and Astronautics (AIAA); 2012. doi:10.2514/6.2003-4187.

[18] García-Cañadas J, Min G. Low frequency impedance spectroscopy analysis of thermoelectric modules. J Electron Mater 2014;43:2411–4. doi:10.1007/s11664-014-3095-4.

[19] Yovanovich M, Tien C, Schneider G. General solution of constriction resistance within a compound disk. 17th Aerosp. Sci. Meet., Reston, Virigina: American Institute of Aeronautics and Astronautics; 1979. doi:10.2514/6.1979-178.

[20] Maillet D, André S, Batsale J-C, Degiovanni A, Moyne C. Thermal Quadrupoles: Solving the Heat Equation through Integral Transforms. New-York: John Wiley and Sons; 2000.

[21] García-cañadas J, Min G. Impedance spectroscopy models for the complete characterization of thermoelectric materials. J Appl Phys 2014;116. doi:10.1063/1.4901213.

[22] Touloukian Y. Thermophysical properties of high temperature solid materials. New York: Macmillan; 1967.

[23] Wolff EG, Schneider DA. Prediction of thermal contact resistance between polished surfaces. Int J Heat Mass Transf 1998;41:3469–82. doi:10.1016/S0017-9310(98)00067-2.

[24] Karthick K, Joy GC, Suresh S, Dhanuskodi R. Impact of Thermal Interface Materials for Thermoelectric Generator Systems. J Electron Mater 2018;47:5763–72. doi:10.1007/s11664-018-6496-y.